Electronic Supplementary Information (ESI):

Exploiting Core/Shell and Core/Alloy Interfaces for Asymmetric Growth of Nanoparticles

Peter N. Njoki, Patrick Lutz, Wenjie Wu, Louis Solomon, Mathew M. Maye*
Department of Chemistry, Syracuse University, Syracuse New York. U.S.A.
mmmaye@syr.edu.

Experimental details:

Materials: Hydrogen tetrachloroaurate (III) hydrate (99.999%), sodium tetrachloropalladate(II) (99.995%), silver nitrate (99.999%), and sodium citrate dihydrate (≥99%), were sourced from Sigma-Aldrich and used as received. Ultrapure water (18.2 MΩ) was obtained from a Sartorius Stedim Arium 61316 reverse osmosis unit combined with an Arium 611DI polishing unit. New 10 mL microwave reaction vessels were obtained from CEM Inc., and first copiously rinsed with ultrapure water before use.

Synthesis of Au/Pd core/shell and Au/Au$_x$Pd$_{1-x}$ core/alloy Cores. The Au/Pd core/shell NPs were synthesized by a procedure recently developed in our lab. *(S1-S2)* We begin with sodium citrate capped Au cores and deposit shells of Pd in controllable layers (*n*). Here, Pd deposition is achieved using a minimum amount of reducing agent, sodium citrate, at microwave mediated hydrothermal temperatures (T_H). The palladium precursors (Na_2PdCl_4) are added and reduced in a step-by-step (e.g. layer-by-layer) fashion at a ratio (r = $[PdCl_4^{2-}]/[Au]$) required to deposit a ~0.50 nm thick shell (t_S), based on model calculations for volume change and core diameter and concentration. The deposition process is then repeated an *n* number of times, resulting in the growth of the Au/Pd core/shell NP. The Au/Pd NPs used in this study at T_H = 120 °C had core + shell diameters (d_{C+S}) of 15.6 ± 1.0 nm (Fig. S1a). The synthesis of core/alloy NPs (Au/Au$_x$Pd$_{1-x}$) were synthesized at elevated T_H = 160 °C. In this case, the alloy rich surface is due to the interdiffusion of core-shell materials, as was previously demonstrated. *(S1)* These NPs had (d_{C+S}) = 16.3 ± 1.0 nm (Fig. S5). Finally, the Au/Au$_x$Pd$_{1-x}$ core/alloy NPs with alloy shell composition of $x = 0.75$ were fabricated by adding an alloy precursor solution at each shell growth (i.e. $AuCl_4^-$ + $PdCl_4^{2-}$) in an analogous way to our recent report for AuAg alloys. *(S2)*

Synthesis of Au/Pd-Ag heterostructures and Au/PdAg NPs: To synthesize the NPs with varied silver (Ag) shells, we begin with either of the Au/Pd cores synthesized above, and deposit shells of Ag in controllable sub nanometer layers (*n*). Here, silver reduction is achieved using sodium citrate (Cit) as the reducing agent. For example, in a typical experiment, a 2.2 mL ultrapure water (18.2 MΩ) solution of Au/Pd ([Au/Pd] = 3.0 nM), trisodium citrate ([Cit]=1.36 mM), and $AgNO_3$ ($[Ag^+]$ = 0.045mM) are hermetically sealed in 10 mL glass microwave reaction vessels. Next, the sample is rapidly heated to hydrothermal temperatures (T_H) and pressures (P_H) using computer controlled microwave irradiation (MWI). A typical reaction time is 3 minutes. After each layer deposition (heating cycle), a 100 uL aliquot was collected for UV-vis and TEM analysis, and a fresh 100 uL aliquot of 1 mM $AgNO_3$ are added. The process is then repeated an *n* number of times, resulting in the growth of the Ag-rich Au/Pd-Ag heterostructure, or the Au/AuPdAg core/alloy NP. Care was taken to perform the experiments under identical conditions, except for the nature of the core interface (i.e., core/shell or core/alloy). No purification was performed in between the deposition steps.

Instrumentation:

Synthetic Microwave Reactor: A Discover-S (CEM Inc) synthetic microwave reactor was employed as the heating source for these experiments. The instrument is computer controlled, and operates at 0-300W and from 30-300 °C. Temperature is monitored in-situ during synthesis via an integrated IR-sensor, or via an immersed fiber optic temperature probe. The instrument is equipped with an active pressure monitoring system, which provides both pressure monitoring and added safety during synthesis. Pressure rated glass reaction vials with volumes of 10 or 35 mL were employed during synthesis. Active cooling was provided by the influx of the MW cavity with compressed N_2, which rapidly cools the sample at a controlled rate.

UV-visible Absorption (UV-vis): The UV-vis measurements were collected on a Varian Cary100 Bio UV-vis spectrophotometer between 200-900nm. The instrument is equipped with an 8-cell automated holder with high precision Peltier heating controller.

Transmission Electron Microscopy (TEM): TEM measurements were performed on either a FEI T12 Twin TEM operated at 120 kV with a LaB6 filament and Gatan Orius dual-scan CCD camera or a FEI T12 Spirit TEM STEM operated at 120 kV equipped with a EDAX Genisis X-ray detector (Cornell Center for Materials Research). Particle size was analyzed manually by modeling each particle as a sphere, with statistical analysis performed using ImageJ software on populations of at least 100 counts. Particle morphology statistics judged by eye.

X-ray Photoelectron Spectroscopy (XPS): XPS also known as electron spectroscopy for chemical analysis (ESCA) measurements were performed on Surface Science Instruments (SSI) model SSX-100 that utilizes monochromated Aluminum K-α x-rays (1486.6 eV) to strike the sample surface (Cornell Center for Materials Research). The analysis depth was ~5nm at an emission angle of 55°. The data was processed using CasaXPS software.

Electrochemical Characterization: Before the electrochemical characterization, the NPs were cleaned by several centrifugations to remove unreacted precursors. Thermal gravimetric analysis (TGA, Q-500 TGA Analyzer) was done to determine the NPs metal concentration in each sample. Carbon black (Vulcan, 30-50 nm) support and was then pretreated by suspending it in ethanol followed by ~ 3 hr sonication at room temperature. A quantitative amount (20 wt%) of NPs was added and the mixture sonicated for ~ 30 min followed by overnight stirring. The resulting carbon-supported NP powders were collected and dried under N_2. The NP/C catalyst ink was made in water/EtOH with 5wt% Nafion, and then quantitatively drop cast onto the surface of cleaned glassy carbon electrodes (GCE), (Ø = 0.3 cm in diameter, exposed geometric surface area 0.07 cm^2, Bioanalytical Systems, Inc., USA). Catalytic activity was probed by cyclic voltammetry (CV) measurements (Galvanostat, PAR-Model 263A) in a three-electrode electrochemical cell at room temperature. All electrolytic solutions were deaerated with high-purity nitrogen before the measurement. The potentials are given with respect to the reference electrode of Ag/AgCl (3.0M KCl).

Supporting Tables & Figures

Table S1: XPS determined compositions of Au/Pd core/shell and Au/Pd-Ag heterostructures prepared at $T_H = 120\ ^oC$.

	XPS Composition		
Sample	**Au (%)**	**Pd (%)**	**Ag (%)**
Au/Pd (core)	20.18	79.82	-
Au/Pd-Ag (*n* = 3)	15.44	66.47	18.09
Au/Pd-Ag (*n* = 5)	14.78	59.13	26.09
Au/Pd-Ag (*n* = 7)	11.67	52.89	35.44
Au/Pd-Ag (*n* = 10)	6.53	40.24	53.23

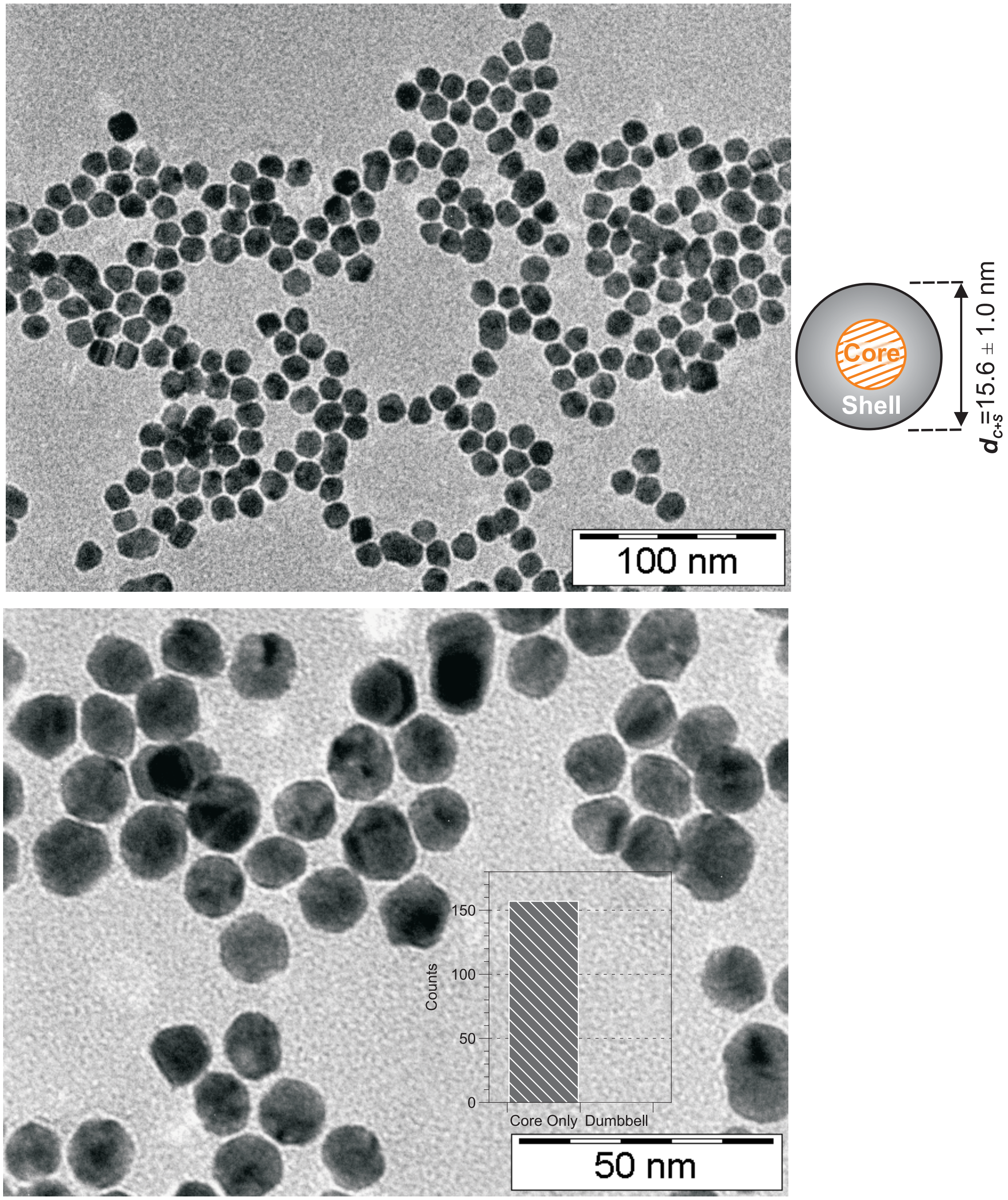

Figure S1: Low magnification TEM images characterizing the morphology of the Au/Pd cores synthesized at T_H = 120 °C with core diameter (d_{C+S}) of 15.6 ± 1.0, before deposition of Ag. Insert: Statistical analysis of dimensions and morphology, revealing a pure population of spherical cores.

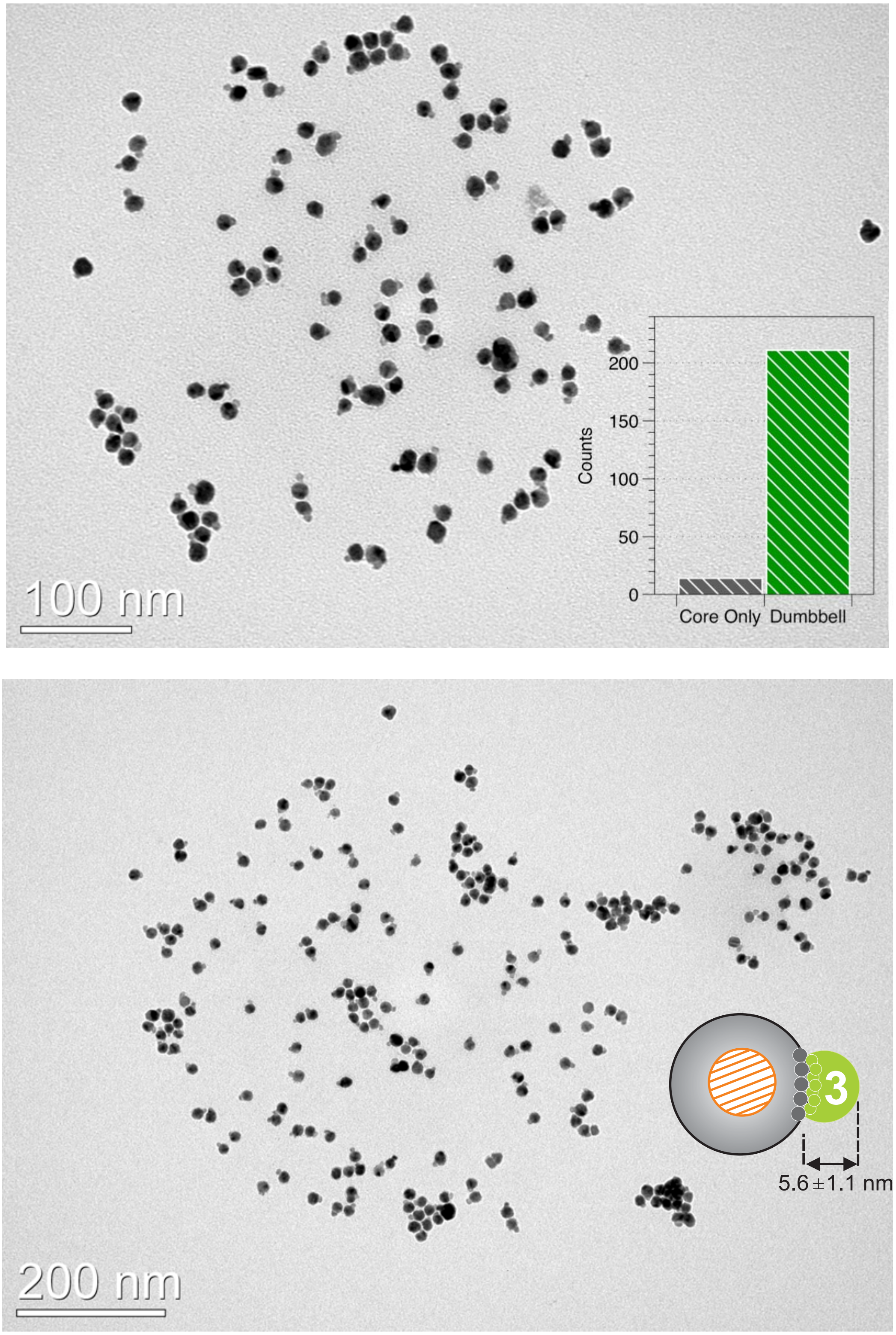

Figure S2: Low magnification TEM images characterizing the morphology of the Au/Pd-Ag heterostructures with Ag deposited at $T_H = 120\ ^oC$ at layers of $n = 3$. Inset: statistical analysis of dumbbell size and morphology population amongst population shown, resulting in 94% dumbbells.

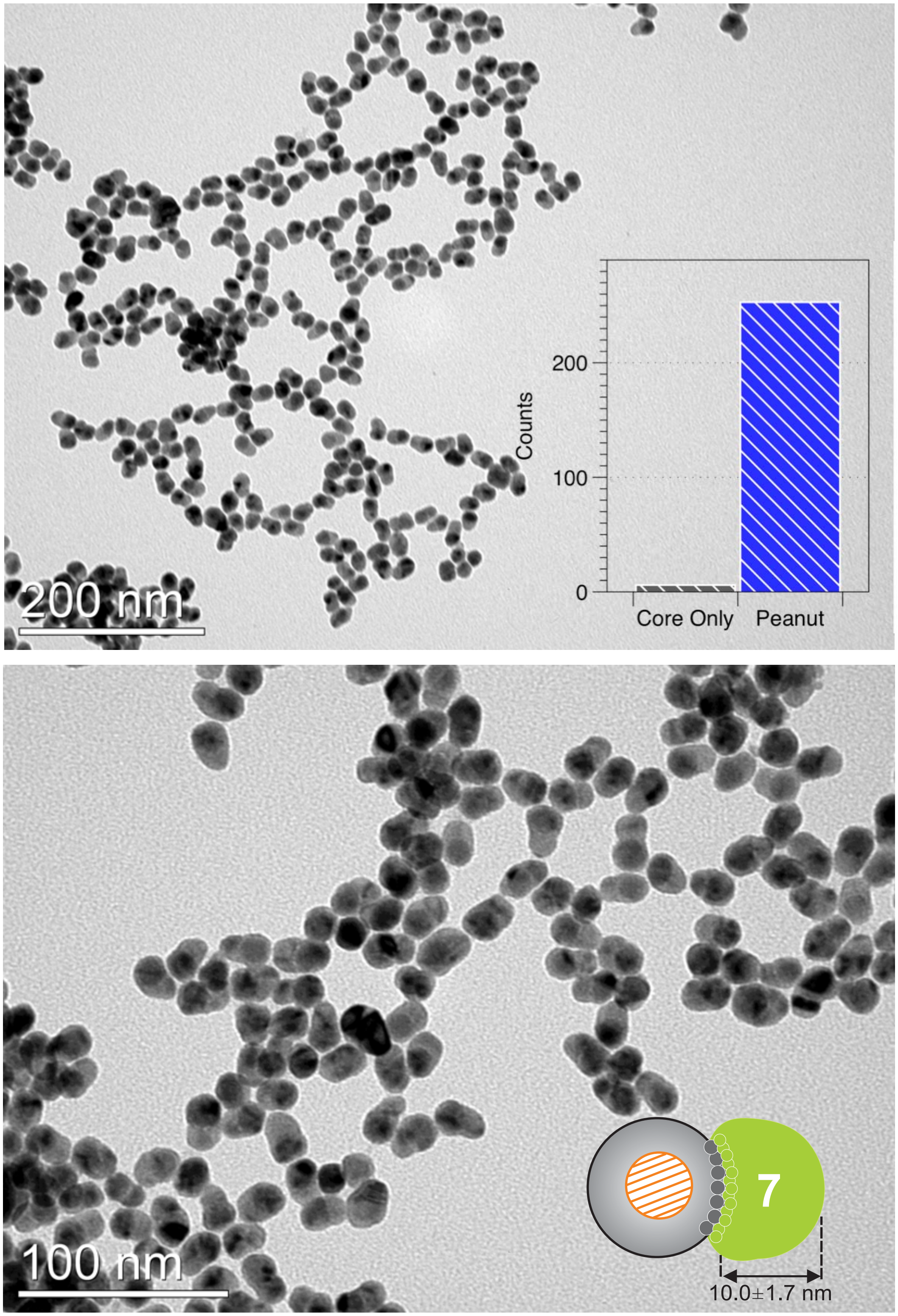

<u>Figure S3:</u> Low magnification TEM images characterizing the morphology of the Au/Pd-Ag heterostructures with Ag deposited at T_H = 120 °C at layers of *n* = 7. Inset: statistical analysis of dumbbell size and morphology population amongst population shown, resulting in 98% peanut shapes.

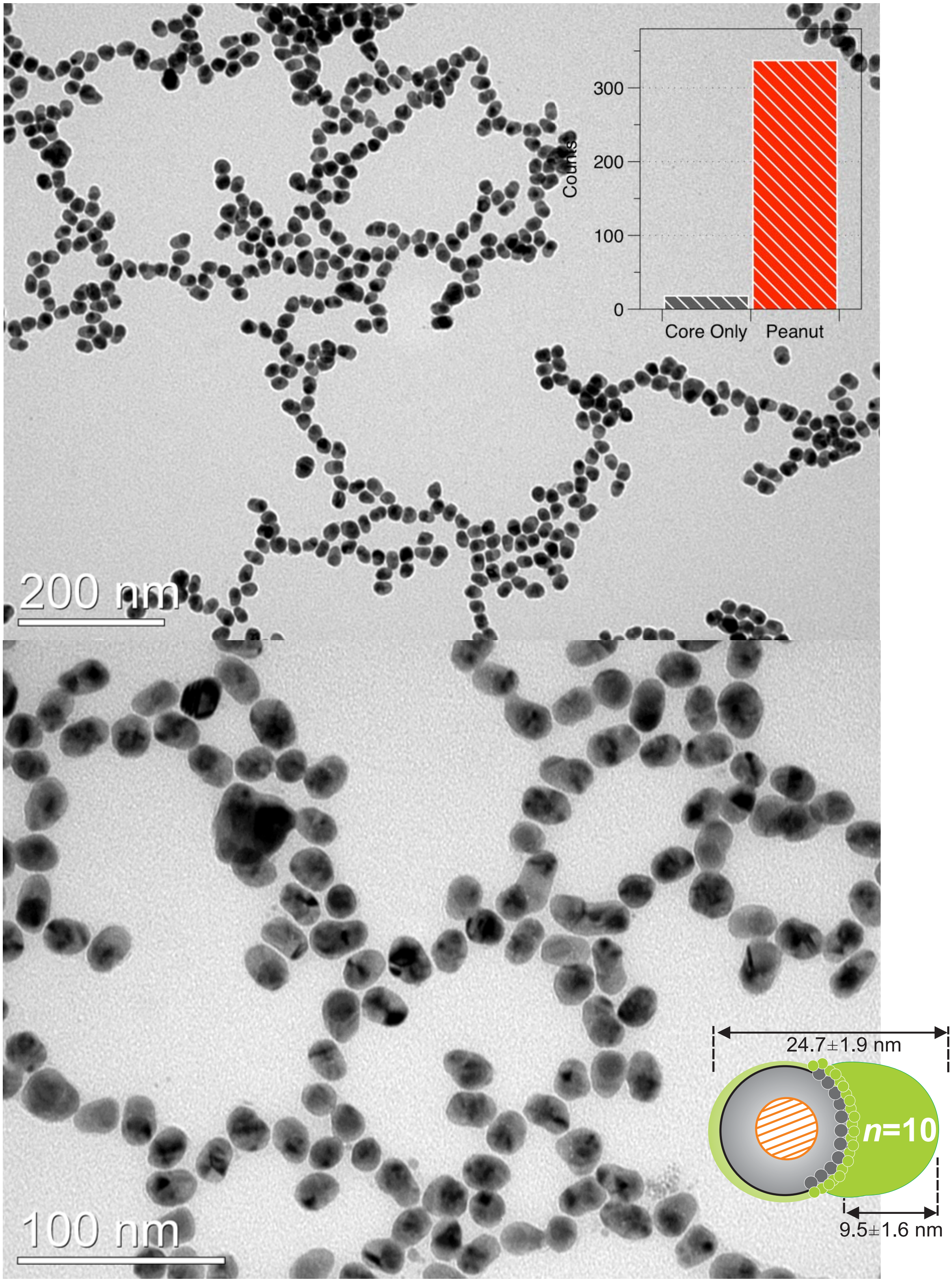

<u>Figure S4</u>: Low magnification TEM images characterizing the morphology of the Au/Pd-Ag heterostructures with Ag deposited at T_H = 120 ^{o}C at layers of *n* = 10. Inset: Statistical analysis of dumbbell size morphology population amongst population shown, resulting in 95% peanut shapes.

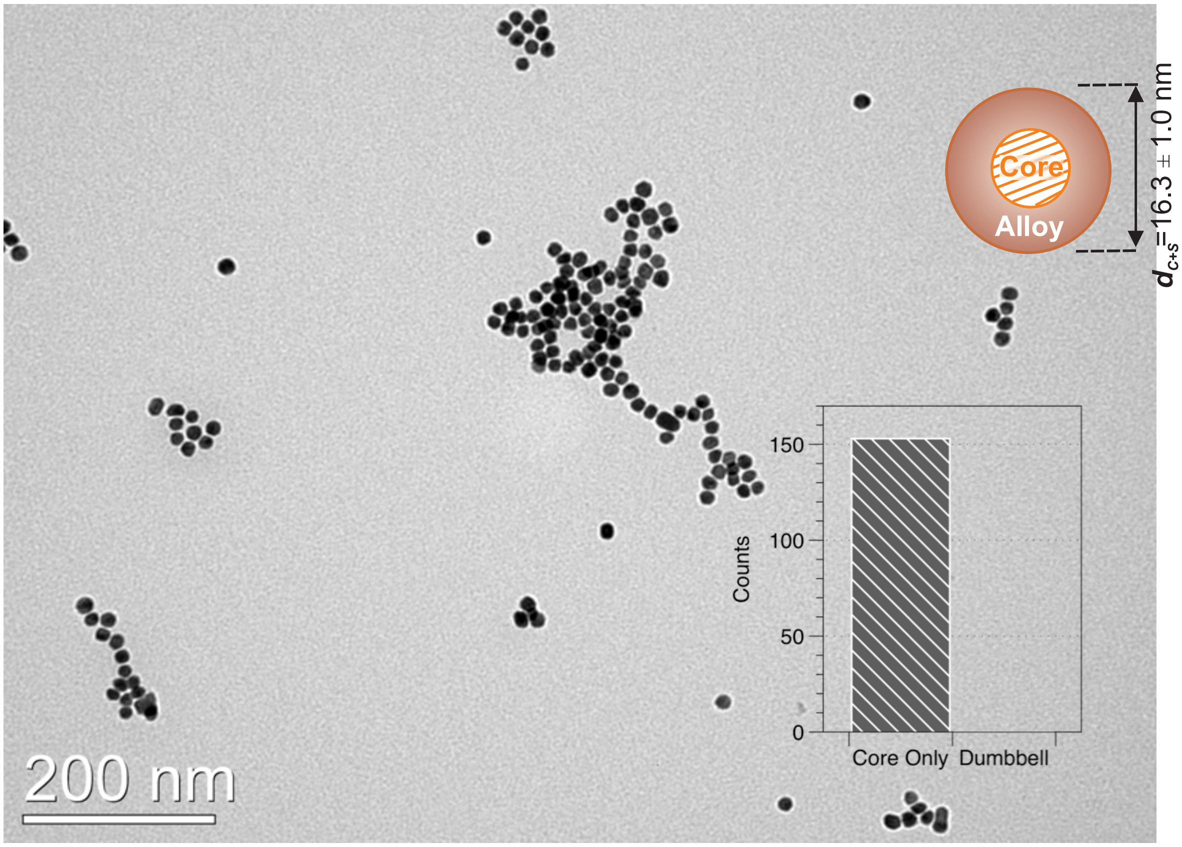

Figure S5: Low magnification TEM images characterizing the morphology of the Au/Au$_x$Pd$_{1-x}$ cores synthesized at T$_H$ = 160 ^{o}C with core diameter (d_C) of 16.3 ± 1.0, before deposition of Ag. Insert: Statistical analysis of morphology revealing a pure population of spherical cores.

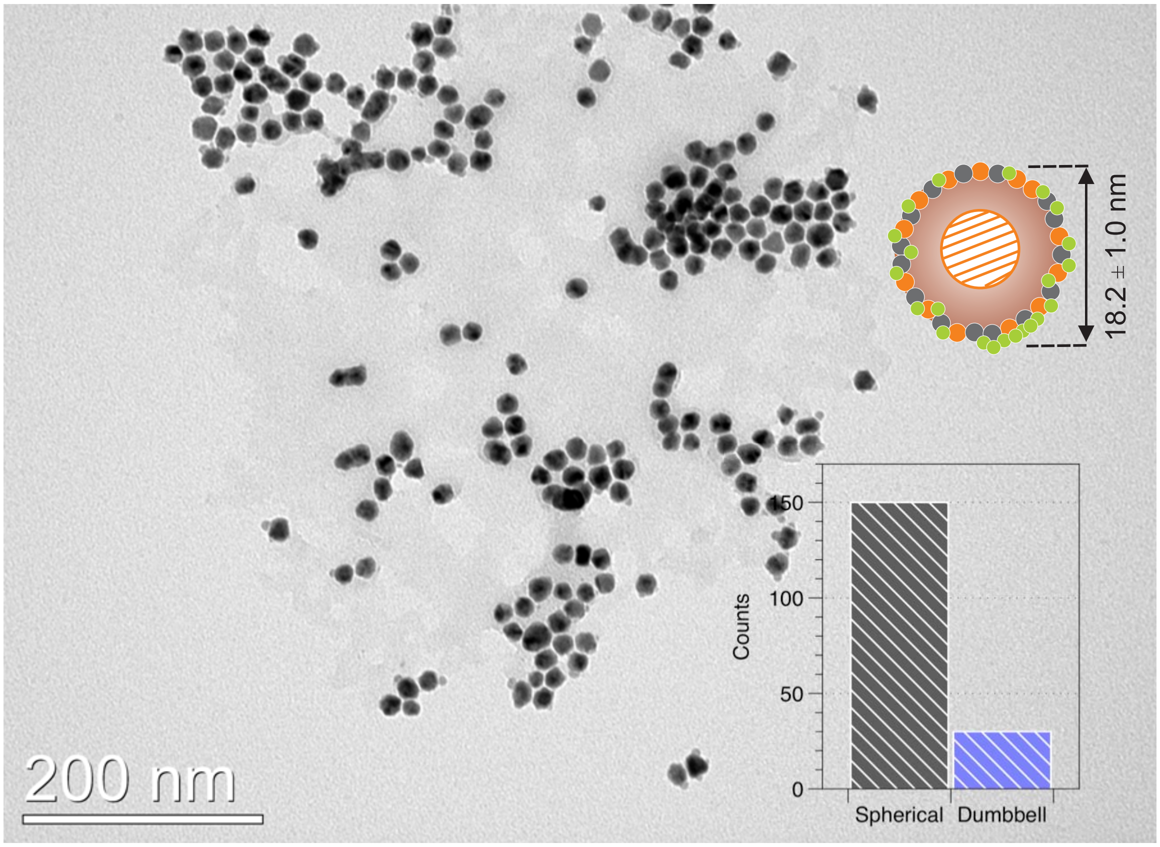

Figure S6: Low magnification TEM images characterizing the morphology of the Au/AuPdAg NPs with Ag deposited at T_H = 160 °C at layers of *n* = 3. Inset: Statistical analysis of morphology population amongst population shown, resulting in 16% asymmetric shapes.

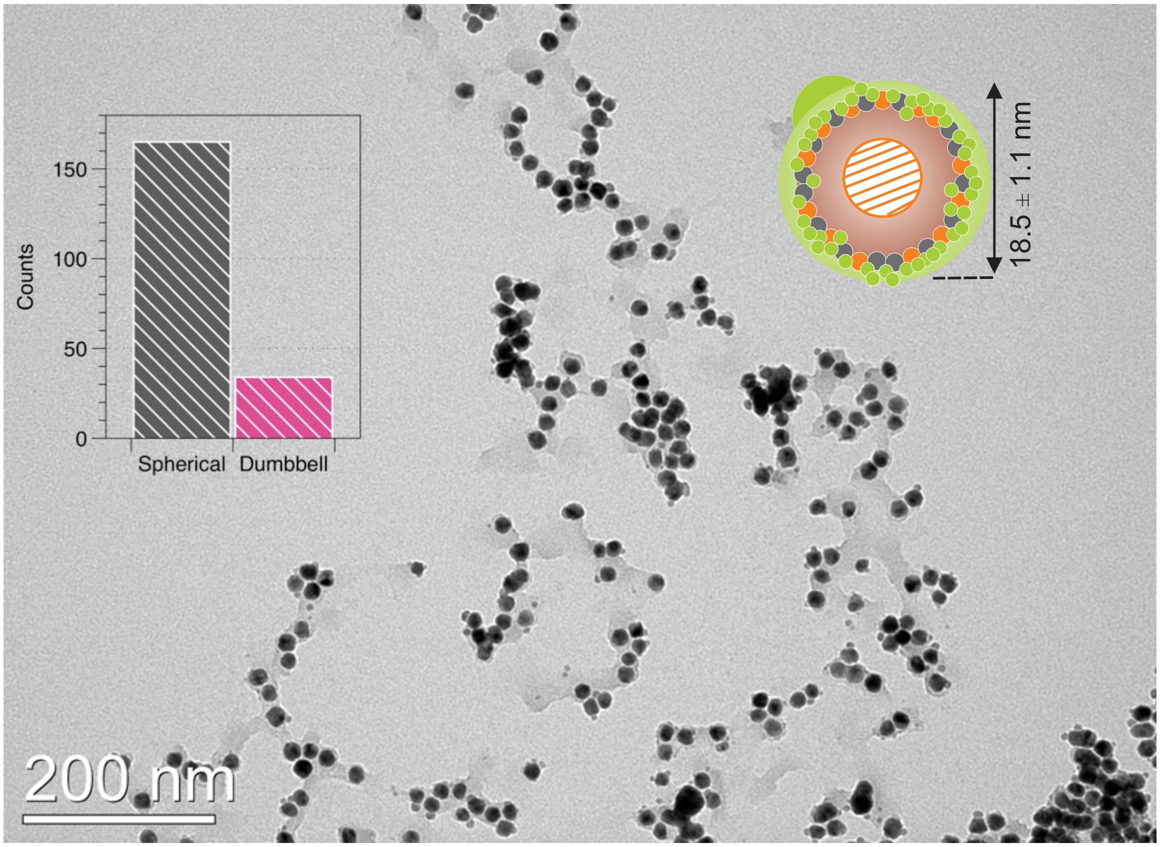

Figure S7: Low magnification TEM images characterizing the morphology of the Au/AuPdAg NPs with Ag deposited at T_H = 160 °C at layers of *n* = 7. Inset: Statistical analysis of morphology population amongst population shown, resulting in 17% asymmetric shapes.

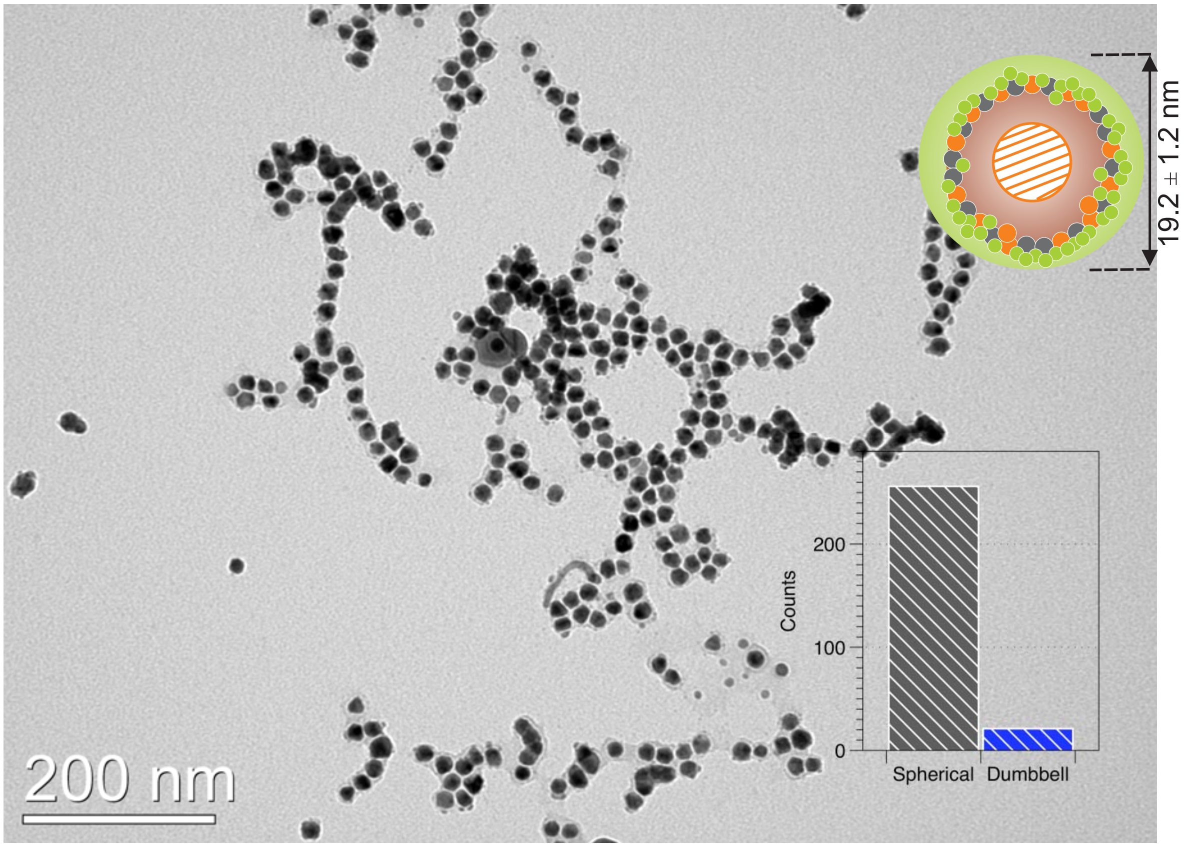

<u>Figure S8</u>: Low magnification TEM images characterizing the morphology of the Au/AuPdAg NPs with Ag deposited at T_H = 160 ^{o}C at layers of n = 10. Inset: Statistical analysis of morphology population amongst population shown, resulting in 7.8% asymmetric shapes.

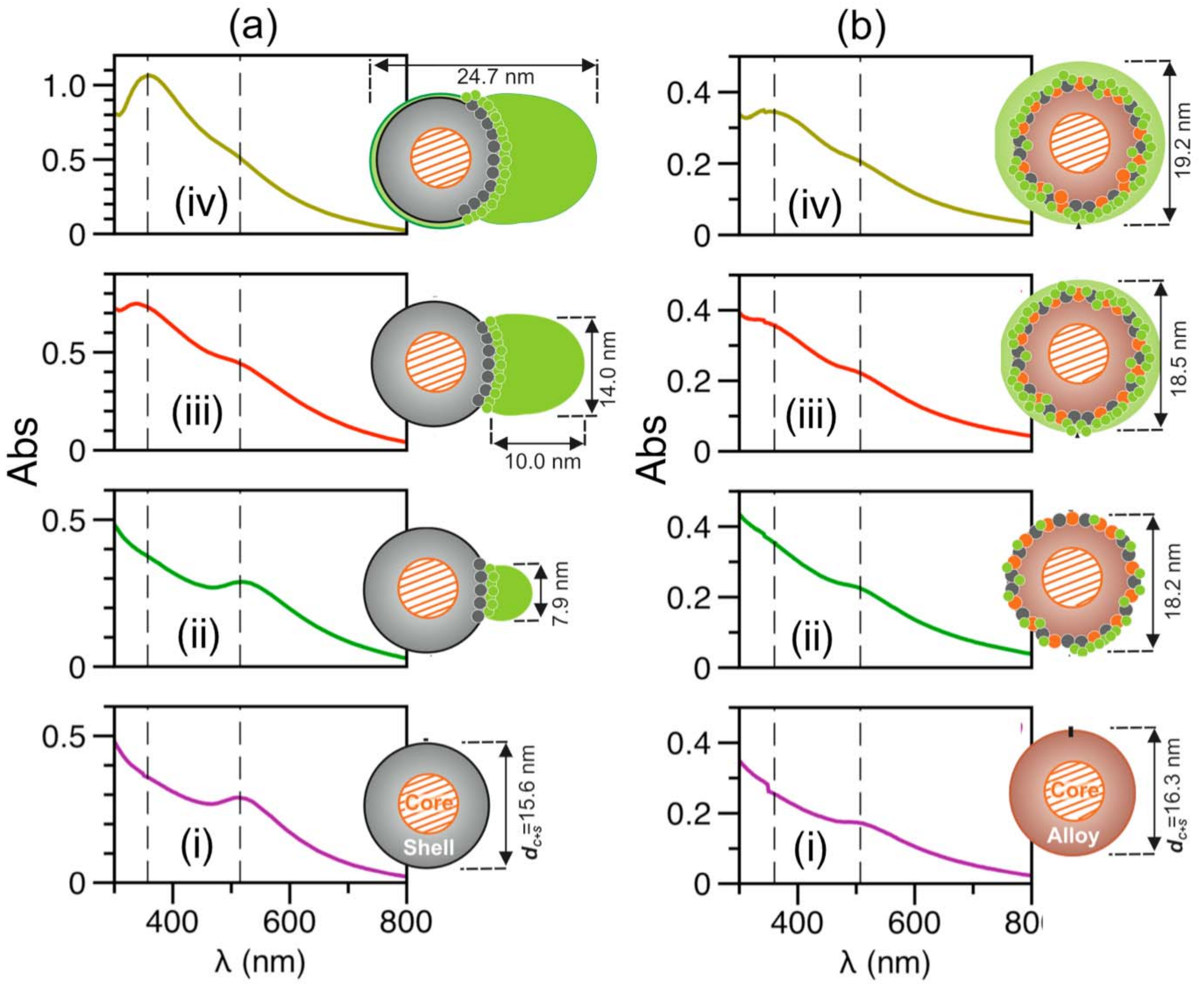

Figure S9: **(a)** Representative UV-vis spectra characterizing the growth of Ag-layers at T_H = 120 ^{o}C on AuPd core/shell NP cores (*i*), and after asymmetric growth of Au/Pd-Ag heterostructures at Ag-layers of *n* = 3 (ii), 7 (iii) and 10 (iv). **(b)** The UV-vis spectra for the growth at elevated T_H = 160 ^{o}C on AuPd core/alloy NP cores (*i*), and after symmetric growth and alloying of Au/PdAg heterostructures at Ag-layers of *n* = 3 (ii), 7 (iii) and 10 (iv). Insets: Schematic illustration of NP morphology and dimensions determined from Fig. 1 and Fig. 2.

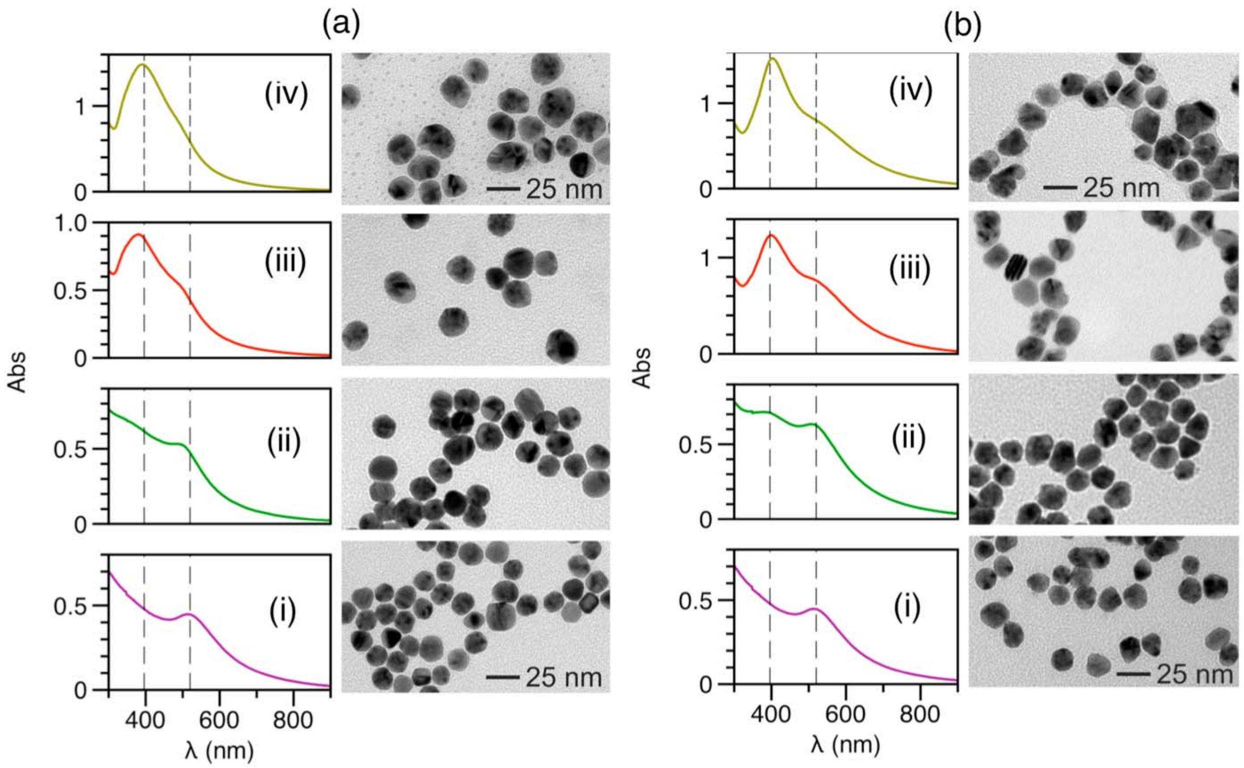

<u>Figure S10</u>: Representative UV-vis spectra and TEM images for the Au/Au$_x$Pd$_{1-x}$ (x = 0.75) core/alloy NP cores (*i*) prepared at T$_H$ = 120 °C **(a)** and 160 ^{o}C **(b),** and after Ag-layer growth at n = 3 (ii), 7 (iii), and 10 (iv). The core + shell diameters (d_{C+S}) of these NP are 17.0 ± 1.0 (a-i), 19.7 ± 1.7 (a-ii), 22.6 ± 1.9 (a-iii), 22.9 ± 3.5 nm (a-iv), 18.1 ± 1.4 (b-i), 19.7 ± 1.4 (b-ii), 22.8 ± 6.0 (b-iii), and 23.0 ± 3.7 nm (b-iv) These control results further confirm the more symmetric growth of Ag at the alloy interface.

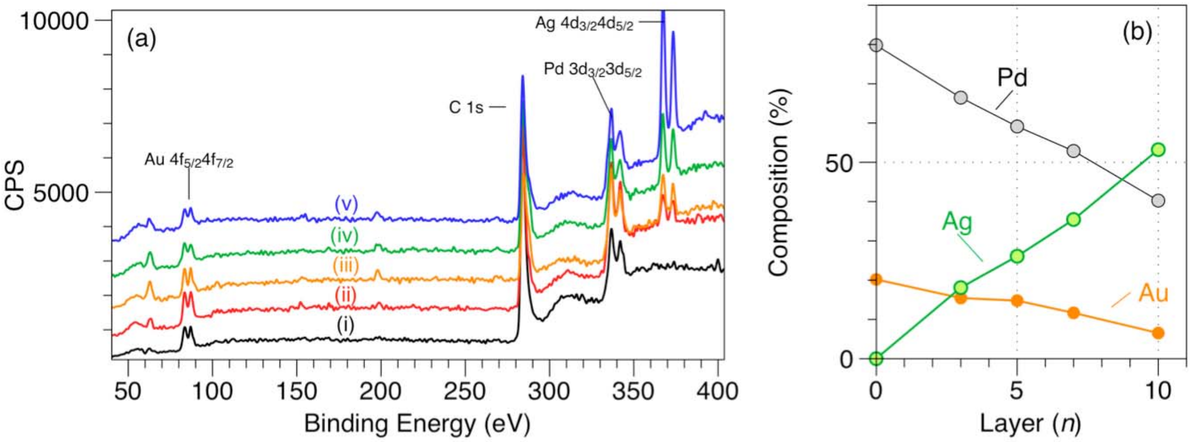

<u>Figure S11</u>: (a) XPS spectra and composition analysis (b) of AuPd core/shell NP cores (i), and after asymmetric growth of Au/Pd-Ag heterostructures at Ag-layers of n = 3 (ii), 5, (iii), 7 (iv), and 10 (v) prepared at T$_H$ = 120 ^{o}C. The XPS samples were prepared by drop casting NPs onto freshly cleaved HOPG substrates. These results demonstrate the increased Ag composition at the NP interface, and the corresponding decrease in %-composition of Au and Pd.

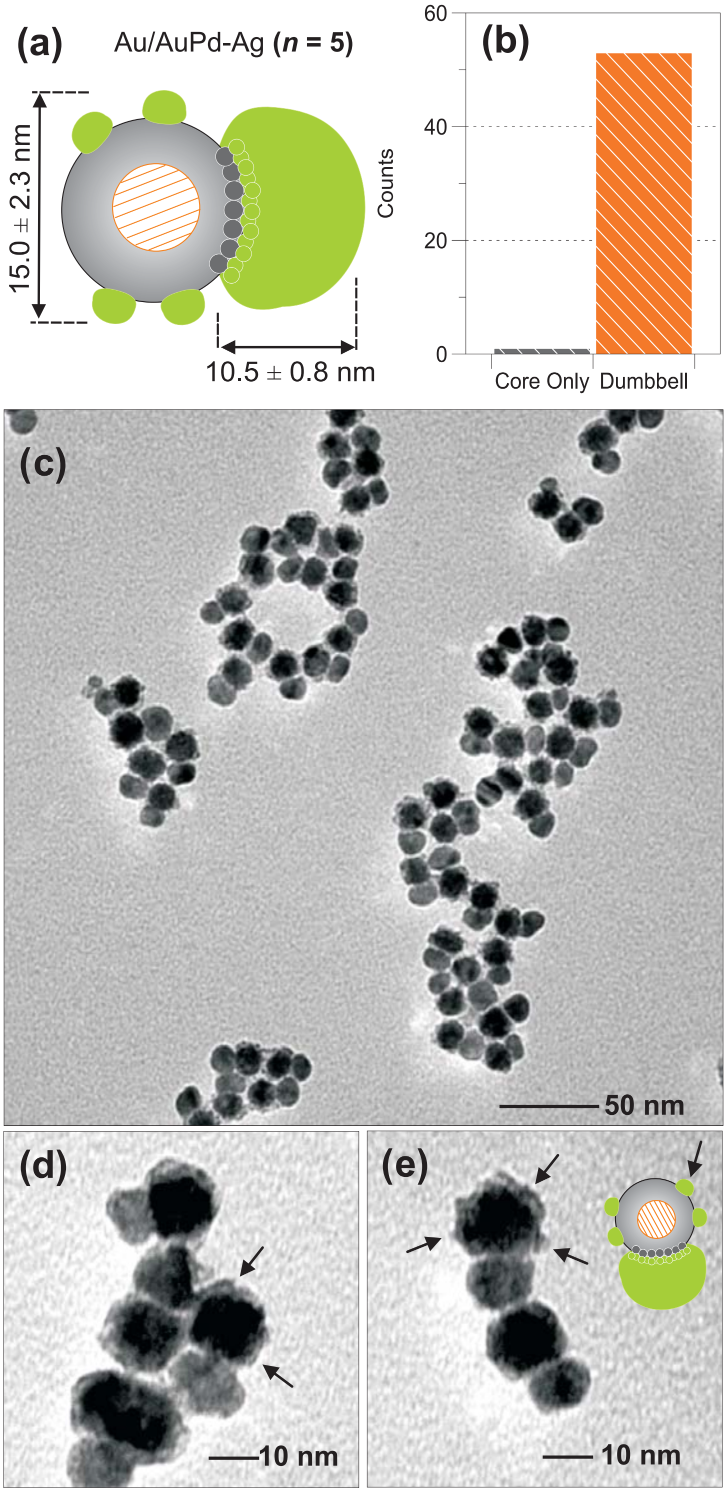

Figure S12: HRTEM images (c-e) of repeat synthesis of Au/Pd-Ag heterostructures with Ag deposited at T_H = 120 ^oC at layer of *n* = 5. The image was analyzed for morphology, statistics of core size, and dumbbell width (a), as well as for dumbbell population (b). These results show the reproducibility of the method, with a different Au/Pd core size of d_C = 12.5 ± 0.9 nm, and reveal that Ag-deposition is shown at the core in a number of dumbbells, as highlighted by the arrow (d-e).

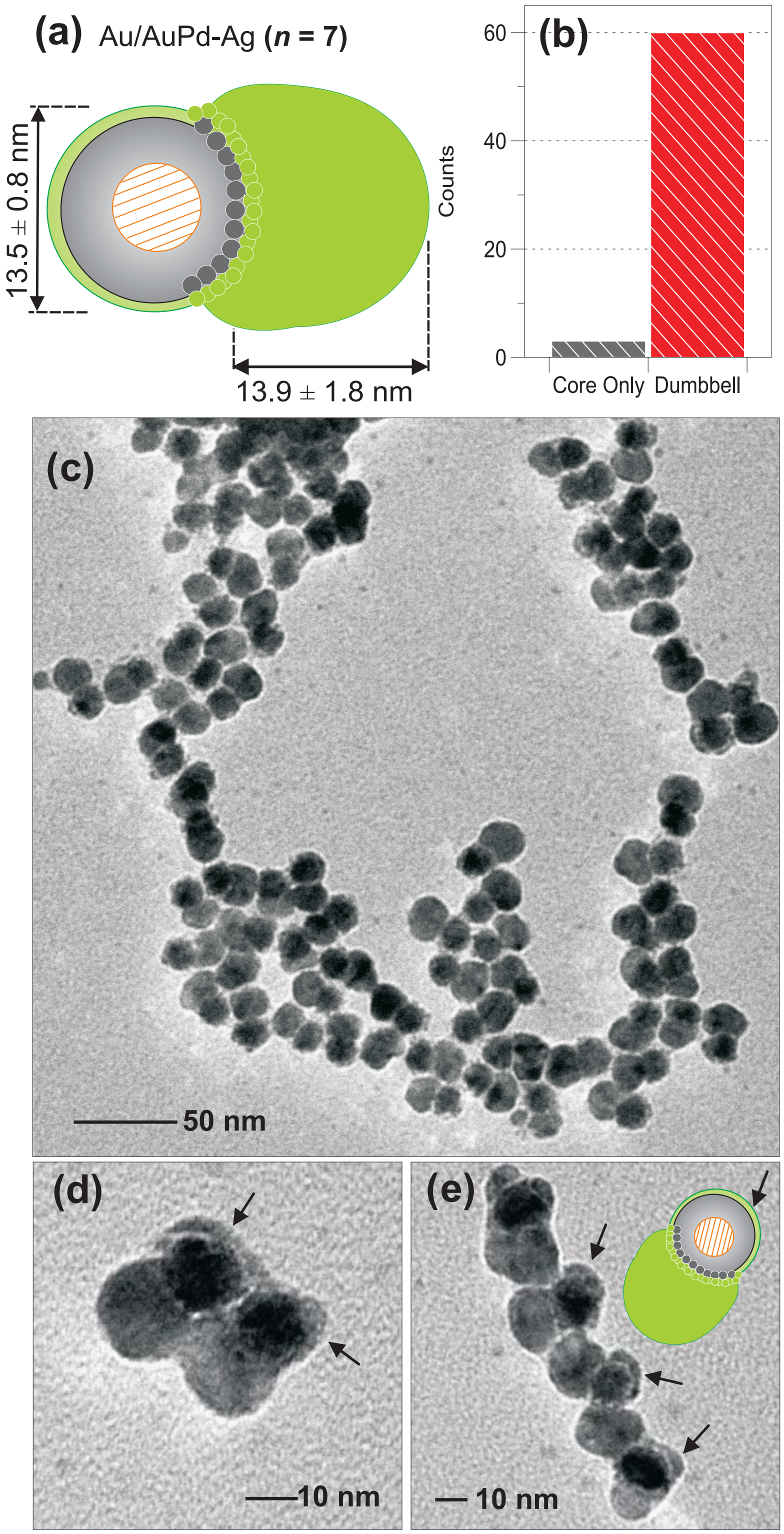

Figure S13: HRTEM images (c-e) of repeat synthesis of Au/Pd-Ag heterostructures with Ag deposited at T_H = 120 ^oC at layer of *n* = 7. The image was analyzed for morphology, statistics of core size, and dumbbell width (a), as well as for dumbbell population (b). These NPs are grown from those shown in Figure S8, and reveal that at n = 7, Ag-deposition begins to coat the core in a more uniform manner (arrows, d-e), and the Ag-dumbbell region continues to grow asymmetrically.

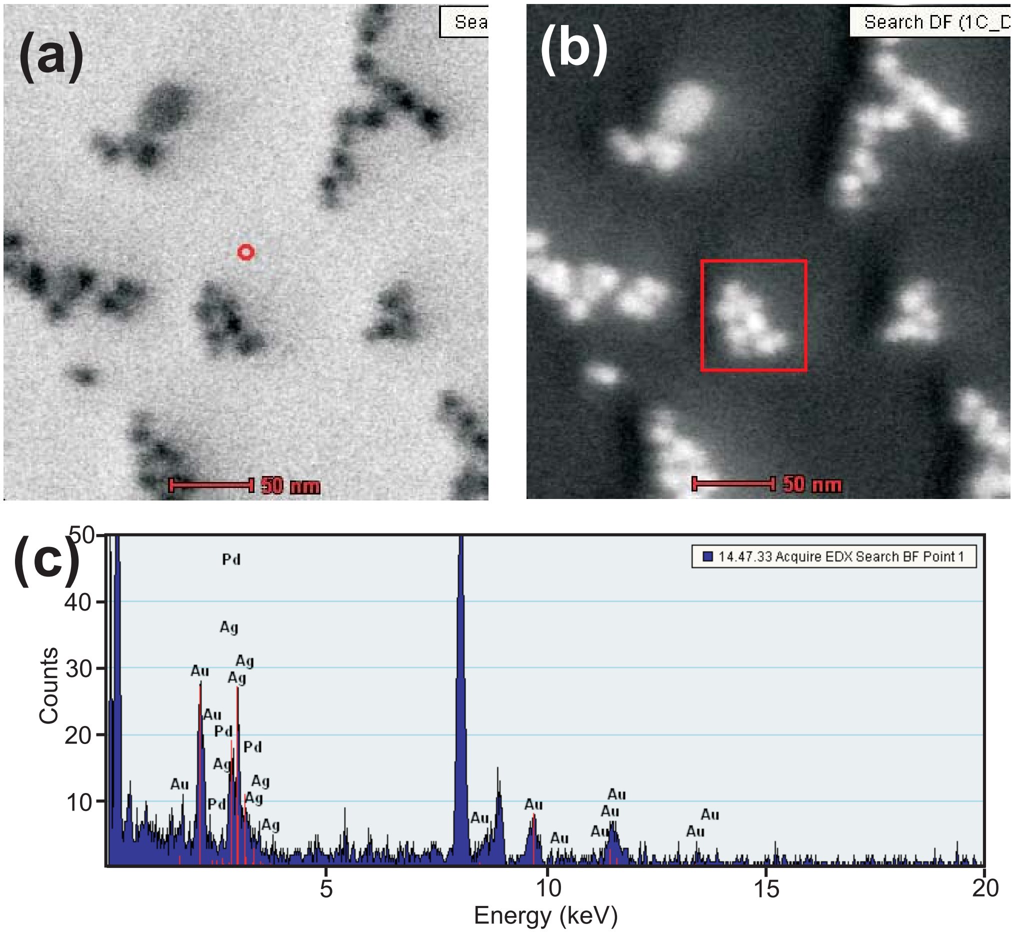

<u>Figure S14:</u> STEM characterization (a-b) of Au/Pd-Ag heterostructures as shown via HRTEM in Figure S12, Ag deposited at T_H = 120 ^{o}C at layer of *n* = 5. Selective area EDX analysis (c) of region shown in b yields characteristic energies of Au, Pd, and Ag. However due to the binding energies of Pd and Ag being largely convoluted, composition determination is challenging. For composition information, XPS results are used, as shown in Figure S11.

Supporting References

S1 P. N. Njoki, L. V. Solomon, W. Wu, R. Alam, M. M. Maye, *Chem. Commun.* 2011, **47**, 10079-10081.

S2 P. N. Njoki, W. Wu, H. Zhao, L. Hutter, E. A. Schiff, M. M. Maye, *J. Am. Chem. Soc.* 2011, **133**, 5224-5227.